Real-complex quantum phase transition in non-Hermitian disorder-free systems

Way Wang[1] and Zhongshui Ma[1,2,*]

[1]*School of Physics, Peking University, Beijing 100871, China*
[2]*Collaborative Innovation Center of Quantum Matter, Beijing 100871, China*

Localization phenomena and the quantum phase transition are two core concepts of low-dimensional condensed-matter physics. The localization transition problem related to vortex line pinning in superconductors can be studied by mapping it to a real-complex non-Hermitian problem. Its relation to the quantum phase transition has to be discerned. We explore these two phase transitions induced by interactions rather than by the disorder in non-Hermitian systems. It is shown that the phase diagram is divided into the classical and quantum regimes by a characteristic temperature. The classical regime contains topological localization transitions and a tricritical point which connects the first-order phase transition line to the second-order transition line. The quantum regime is a nonchaotic and first-order phase transition. In such a quantum regime, the relaxation time does not always satisfy the bound on chaos. We show that the oscillation phase transition line due to quantized Matsubara frequencies can give an index similar in structure to the quantum oscillation in an imaginary magnetic field, which makes the first-order quantum phase diagram behave as a quantum critical phase diagram.

I. INTRODUCTION

Since the problem of localization on vortex line pinning in superconductors was studied by mapping to a non-Hermitian system [1], the real-complex transition [2], distinguished as a localization-delocalization transition, has been investigated in various disordered non-Hermitian systems [3–7]. So far the disorder has been considered to play a pivotal role in such transitions [8,9]. Whether the disorder is a precondition [10] for the real-complex transition and what kind of characteristic behavior will emerge at $T \to 0$ are core issues worth in-depth exploration. Especially for the zero-temperature limitation, the phase transition [11] is dominated by quantum fluctuations rather than driven by temperature. The second-order quantum phase transition (QPT), which is also known as a quantum critical phenomenon (QCP) [12], has received extensive attention. Because it can influence the properties of materials in a wide range of temperatures, not just at the theoretical zero temperature, which is impossible, it provides a different perspective for exploring the fascinating properties of heavy-fermion compounds [13], cuprates [14], and graphene with interaction [15]. Interestingly, studies have found that some QCPs might be destroyed by genetic soft modes, so then the phase transition would change from second order to first order, which is known as the Coleman-Weinberg mechanism [16]. It has been used to explain [17] why the paramagnetic-ferromagnetic transition, which was suggested theoretically to be second order, becomes a first-order phase transition in actual clean materials [18–20]. A transition converted from first order to second order has been discovered in long-range interaction systems [21]. These two kinds of transition lines

in the conversion process are usually linked by a tricritical point (TCP) [22,23]. Such topics, up to now, have been discussed abundantly for Hermitian systems, but to the best of our knowledge, there is a lack of research on non-Hermitian systems [24,25].

The non-Hermitian Hamiltonian, which breaks the conservation law, is usually used to describe open systems [26]. Correlative studies can be dated back to Gamow [27] and Feshbach [28]. Although the non-Hermitian Hamiltonian usually has complex eigenvalues, it can present real eigenvalues due to the PT symmetry [24] or pseudo-Hermiticity [25]. In common non-Hermitian systems, the quasiparticles in the usual sense are ill defined because of the lack of a Fermi surface and creation-annihilation operators. A similar situation may occur in Hermitian strongly correlated systems whose spectrum function width is comparable to $k_B T$ [29], such as overdoped cuprates [30], quantum critical regimes [12], and so on. But for real eigenstates whose lifetimes are infinite, we can even map them to Hermitian systems with the same eigenvalues as quasi-Hermitian systems [31]. The concept of quasiparticles is then revived to some extent. Here the real-complex transition is not merely a localization-delocalization transition but also a transition from quasiparticles to nonquaisparticles. A good understanding of the latter phase transition may help us to understand the transition from the non-Fermi to Fermi liquid in strongly correlated systems. Therefore, it is crucial to unveil the intriguing relation between the real-complex transition and the quantum phase transition, especially in disorder-free systems.

In this paper, we study the localization phenomena and quantum phase transition in non-Hermitian quantum systems. The real-complex transition in disorder-free systems is revealed for different temperatures, including the theoretical zero-temperature limit, i.e., the quantum phase transition.

*Corresponding author: mazs@pku.edu.cn

TABLE I. Types of real-complex transitions at different energy scales.

Phase diagram	Classical regime				Quantum regime		
Transition temperature T_t [a]		$T_t > T_c$			$T_t = T_c$	$T_t < T_c$	$\lim T_t \to 0$
Relaxation time τ_s		$\tau_s \geqslant \frac{\hbar}{2\pi k_B T_t}$			$\tau_s \geqslant \frac{\hbar}{2\pi k_B T_c}$	τ_s ?[b] $\frac{\hbar}{2\pi k_B T_t}$	$\frac{\hbar}{2\pi k_B T_t} \to \infty$
Types of phase transitions	nontopological		topological			first-order[c]	quantum phase transition
	real-complex (point gapped phase $\Leftrightarrow$ normal phase)		real-complex	real-real[d]	no phase transition	real-complex	real-complex
	$T_t > T_{TCP}$, second-order	$T_t = T_{TCP}$[e], tricritical point	$T_t < T_{TCP}$, first-order	(point gapped phase $\Leftrightarrow$ gapless phase)	(line gapped phase $\Leftrightarrow$ gapless phase)		(line gapped phase $\Leftrightarrow$ normal phase)	(line gapped phase $\Leftrightarrow$ normal phase), transition point U_c [f]

[a]The transition temperature T_t corresponds to the temperature on the transition lines.
[b]The question mark(?) means no defined inequality relation.
[c]Boundaries of oscillation line satisfy the scaling law.
[d]It is also a continuous metal-insulator transition.
[e]T_{TCP} is the temperature at the TCP.
[f]At this point the order parameter has no defined value.

Corresponding phase transitions are summarized in Table I. As a result, a characteristic temperature T_c is emphasized. By comparing it with the transition temperature T_t (the temperature that corresponds to the transition lines), the phase diagram can be divided into classical and quantum regimes. The division is determined by the lower bound of quantum chaos [32] for the relaxation time $\hbar/(2\pi k_B T_c)$. One obvious feature is that the lower bound is not always satisfied in the quantum regime. We call it nonquantum chaotic [33] for this reason. What is more, in the classical regime ($T_t > T_c$), the real-complex transitions are characterized by two different phase transitions, topological and nontopological phase transitions. For the topological phase transition, it could be a transition either from the real spectrum to the complex spectrum or between the pure real spectrums with an energy gap opened or closed. The latter is exactly the continuous metal-insulator transition. For the nontopological phase transition, it contains a nontrivial tricritical point at which the second-order phase transition line and the first-order phase transition line converge. Beyond that, in the quantum regime ($T_t < T_c$), it is found that the first-order transition line oscillates with a period proportional to $1/T$. Such oscillations can be identified as the non-Hermitian version of quantum oscillation in an imaginary magnetic field by replacing the quantized Landau levels with Matsubara frequencies. The regime is characterized by an oscillation crossover region. Its phase diagram manifests as the quantum critical phenomenon, in which the order parameter oscillates between zero and finite values, and it has no definite value at the zero temperature. In the Hermitian limitation, $T_c = 0$, the quantum regime discussed no longer exists.

This paper is organized as follows. In Sec. II, we explore the general Hamiltonian and stress the interaction induced by the dipole hopping [34] term, which becomes important due to the non-Hermitian skin effect. Using the path integral method under the mean-field approximation, the gap equation and condensed energies are obtained, the negative values of which ensure the stability of transition. In Sec. III the bilayer Nelson-Hatano model is investigated. The spectrum and thermodynamic properties are calculated. The corresponding phase characteristic is revealed, and the QPT and quantum chaotic behavior are discussed. The conclusions are given in Sec. IV.

II. FUNDAMENTAL FORMALISM

The non-Hermiticity of electrons located near the open boundary mirrors the non-Hermitian skin effect [35–44]. We construct a bilayer non-Hermitian system with interaction induced by the dipole hopping, as shown in Fig. 1, in which the imaginary parts of two layers have opposite signs. The electrons locate on different sides of the upper and lower layers, while the holes locate on the facing sites vertically. It is shown that the term is obtained by the subscripts of centrosymmetrical sites rather than the normal direct and exchange terms. The exciton then plays a crucial part in constructed bilayer systems [45]. The system is described by the Hamiltonian $H = H_0 + H_d$, where H_0 is the free Hamiltonian,

$$H_0 = \sum_{\boldsymbol{k},\sigma}^{BZ}[h_{\sigma,u}(\boldsymbol{k})c_{\boldsymbol{k},\sigma,u}^{\dagger}c_{\boldsymbol{k},\sigma,u} + h_{\sigma,l}(\boldsymbol{k})c_{\boldsymbol{k},\sigma,l}^{\dagger}c_{\boldsymbol{k},\sigma,l}], \quad (1)$$
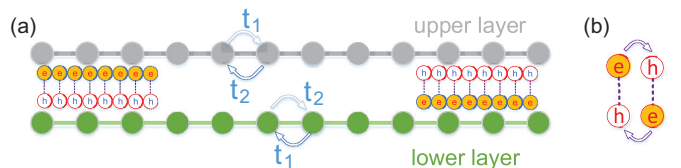

FIG. 1. Sketch of the bilayer Nelson-Hatano model. (a) Bilayer non-Hermitian systems with opposite imaginary parts in different layers. Due to the non-Hermitian skin effect, electrons locate on different sides of the upper and lower layers, while the holes locate at the facing sites vertically. (b) The interaction produced by exciton hopping.

and H_d is the major hopping term for an interlayer exciton induced by Coulomb interaction [46–48],

$$H_d = -\frac{U}{N} \sum_{k_1,k_2,\sigma}^{\mathrm{BZ}} c^\dagger_{k_1,\sigma,u} c_{k_1,\sigma,l} c^\dagger_{k_2,\sigma,l} c_{k_2,\sigma,u}. \tag{2}$$

BZ is the Brillouin zone, $c_{k,\sigma,u/l}$ and $c^\dagger_{k,\sigma,u/l}$ are the annihilation and creation operators of the electron in k-momentum space with spin $\sigma(=\uparrow,\downarrow)$, u and l denote the upper and lower layers, and N is the number of lattice sites. $h_{\sigma,u}(\boldsymbol{k})$ and $h_{\sigma,l}(\boldsymbol{k})$ in H_0 are the energy dispersion relations on two layers, U in H_d is the interaction strength, and the negative sign indicates that two antiparallel dipole moments attract each other. A similar interaction can also be found for monolayer non-Hermitian systems. In Appendix A, we show that a similar term can be derived from the Coulomb interaction in the Wannier bases.

The partition function is defined as $\mathcal{Z} = \mathrm{Tr}\, e^{-\beta H}$ [49–53], where the trace with fermion coherent states [49] is employed. The imaginary-time partition function of the system can be written as

$$\mathcal{Z} = \int \mathcal{D}[c^\dagger_k(\tau), c_k(\tau)] \exp\left(-\int_0^\beta d\tau \mathcal{L}\right), \tag{3}$$

where the Lagrangian is given by

$$\mathcal{L} = \sum_{k,\sigma,\lambda(=l,u)}^{\mathrm{BZ}} c^\dagger_{k,\sigma,\lambda}(\tau) \partial_\tau c_{k,\sigma,\lambda}(\tau) + H_0 + H_d, \tag{4}$$

and the temperature $(\sim 1/\beta)$ is well defined as a real scalar, which is different from the normal non-Hermitian system [54]. The partition function is real because the eigenenergies are real or appear in pairs as a conjugate complex with the same degeneracy [50,55].

By performing a Hubbard-Stratnovich transformation with auxiliary fields Δ and Δ^*, the attractive interactions $(U > 0)$ in the exciton channels are decoupled as

$$\exp\left(\int_0^\beta d\tau \frac{U}{N} \sum_{\sigma,k_1,k_2} c^\dagger_{k_1,\sigma,u} c_{k_1,\sigma,l} c^\dagger_{k_2,\sigma,l} c_{k_2,\sigma,u}\right)$$

$$= \int \mathcal{D}[\Delta^*,\Delta] \exp\left\{\int_0^\beta d\tau\left(-2|\Delta|^2 \frac{N}{U}\right.\right.$$

$$\left.\left.-\Delta \sum_{k,\sigma} c^\dagger_{k,\sigma,u} c_{k,\sigma,l} - \Delta^* \sum_{k,\sigma} c^\dagger_{k,\sigma,l} c_{k,\sigma,u}\right)\right\}. \tag{5}$$

Meanwhile, in order to facilitate the summation method of Matsubara frequencies, we write the partial function into the frequency space by using the relations $c_k(\tau) = (1/\sqrt{\beta}) \sum_{\omega_n} e^{-i\omega_n\tau} c_k(\omega_n)$, $c^\dagger_k(\tau) = (1/\sqrt{\beta}) \sum_{\omega_n} e^{i\omega_n\tau} c^\dagger_k(\omega_n)$, $\Delta(\tau) = (1/\sqrt{\beta}) \sum_{\Omega_n} e^{-i\Omega_n\tau} \Delta(\Omega_n)$, $\Delta^*(\tau) = (1/\sqrt{\beta}) \sum_{\Omega_n} e^{i\Omega_n\tau} \Delta^*(\Omega_n)$, and $\int_0^\beta d\tau e^{-i\omega_n\tau} = \beta\delta_{\omega_n,0}$. We obtain

$$\mathcal{Z} = \int \mathcal{D}[c^\dagger(\omega_n), c(\omega_n), \Delta^*(\Omega_n), \Delta(\Omega_n)]$$

$$\times \exp\left\{-\sum_{k,\sigma,\omega_n}^{\mathrm{BZ}} [(-i\omega_n + h_k)c^\dagger_{k,\sigma,u}(\omega_n) c_{k,\sigma,u}(\omega_n)\right.$$

$$+ (-i\omega_n + h_k^*)c^\dagger_{k,\sigma,l}(\omega_n) c_{k,\sigma,l}(\omega_n)] - \frac{2N}{U} \sum_{\Omega_n} |\Delta(\Omega_n)|^2$$

$$- \sum_{k,\sigma,\omega_n,\Omega_n}^{\mathrm{BZ}} \left(\frac{\Delta(\Omega_n)}{\sqrt{\beta}}[c^\dagger_{k,\sigma,u}(\omega_n + \Omega_n) c_{k,\sigma,l}(\omega_n)]\right.$$

$$\left.\left.+ \frac{\Delta^*(\Omega_n)}{\sqrt{\beta}}[c^\dagger_{k,\sigma,l}(\omega_n) c_{k,\sigma,u}(\omega_n + \Omega_n)]\right)\right\}. \tag{6}$$

Next, we will take the mean-field approximation in which $\Delta(\Omega_n) = \sqrt{\beta}\Delta\delta_{\Omega_n,0}$ and $\Delta^*(\Omega_n) = \sqrt{\beta}\Delta^*\delta_{\Omega_n,0}$. In this way, the partition function in frequency space can be written as $\mathcal{Z} = \int \mathcal{D}[c^\dagger(\omega_n), c(\omega_n), \Delta^*, \Delta]e^{-S}$, where

$$S = \sum_{k,\sigma,\omega_n}^{\mathrm{BZ}} \xi^\dagger_{k,\sigma}(-i\omega_n I + H_k)\xi_{k,\sigma} + \frac{2\beta N}{U}|\Delta|^2, \tag{7}$$

$H_k = \begin{pmatrix} h_k & \Delta \\ \Delta^* & h_k^* \end{pmatrix}$, $\xi_{k,\sigma}(\omega_n) = (c_{k,\sigma,u} \quad c_{k,\sigma,l})^{\mathcal{T}}$, $\mathcal{T}$ indicates the transposition, and ω_n is the Matsubara frequency. Correspondingly, the mean-field Hamiltonian reads

$$H_{\mathrm{mean}} = \sum_{k,\sigma}^{\mathrm{BZ}} \xi^\dagger_{k,\sigma} H_k \xi_{k,\sigma} + \frac{2N}{U}|\Delta|^2, \tag{8}$$

which, in fact, can also be elucidated by substituting $c^\dagger_{k,\sigma,u} c_{k,\sigma,l} = -(N/U)\Delta^* + \delta(c^\dagger_{k,\sigma,u} c_{k,\sigma,l})$ and neglecting terms higher than second order δ^2.

The eigenenergy spectrum is

$$\varepsilon_{k,\sigma,\pm} = \mathrm{Re}\, h_{k,\sigma} \pm \Sigma_{k,\sigma}(\Delta), \tag{9}$$

with

$$\Sigma_{k,\sigma}(\Delta) = \sqrt{|\Delta|^2 - (\mathrm{Im}\, h_{k,\sigma})^2}. \tag{10}$$

Equations (9) and (10) show that the eigenenergies are complex with finite real and imaginary parts for $|\Delta| < \min|\mathrm{Im}\, h_k|$ and purely real for $|\Delta| > \max|\mathrm{Im}\, h_k|$. This reflects the fact that, when we change $|\Delta|$ by modulating the temperature or the strength of interaction, a real-complex transition of the spectrum can be expected. The Hamiltonian in Eq. (8) can then be written in terms of the annihilation and creation operators of non-Hermitian quasiparticles $\alpha_{k,\sigma}, \gamma_{k,\sigma}, \alpha^\ddagger_{k,\sigma}$, and $\gamma^\ddagger_{k,\sigma}$ as

$$\xi^\dagger_{k,\sigma} H_k \xi_{k,\sigma} = \varepsilon_{k,\sigma,+}\alpha^\ddagger_{k,\sigma}\alpha_{k,\sigma} + \varepsilon_{k,\sigma,-}\gamma^\ddagger_{k,\sigma}\gamma_{k,\sigma}, \tag{11}$$

where $\alpha^\ddagger_{k,\sigma}$ and $\gamma^\ddagger_{k,\sigma}$ and $\alpha_{k,\sigma}$ and $\gamma_{k,\sigma}$ relate $\xi_{k,\sigma}$ and $\xi^\dagger_{k,\sigma}$ by the non-Hermitian Bogoliubov transformations

$$\begin{pmatrix} \alpha_{k,\sigma} \\ \gamma_{k,\sigma} \end{pmatrix} = \Xi_{k,\sigma}\xi_{k,\sigma} \tag{12}$$

and

$$(\alpha^\ddagger_{k,\sigma} \quad \gamma^\ddagger_{k,\sigma}) = \xi^\dagger_{k,\sigma}\Xi_{k,\sigma}, \tag{13}$$

respectively, and

$$\Xi_{k,\sigma} = [2i\Sigma_{k,\sigma}(\mathrm{Im}\, h_{k,\sigma} - i\Sigma_{k,\sigma})]^{-1/2}$$

$$\times \begin{pmatrix} h_{k,\sigma} - \varepsilon_{k,\sigma,-} & \Delta \\ \Delta^* & h^*_{k,\sigma} - \varepsilon_{k,\sigma,+} \end{pmatrix}. \tag{14}$$

Although the annihilation operators of non-Hermitian quasiparticles are not the Hermitian conjugate of their creation operator [54,56] $\begin{pmatrix} \alpha_{k,\sigma} \\ \gamma_{k,\sigma} \end{pmatrix}^{\dagger} \neq (\alpha_{k,\sigma}^{\ddagger} \quad \gamma_{k,\sigma}^{\ddagger})$, they do satisfy the anticommutation relations as follows: $\{\alpha_{k,\sigma}, \alpha_{k',\sigma'}^{\ddagger}\} = \{\gamma_{k,\sigma}, \gamma_{k',\sigma'}^{\ddagger}\} = \delta_{kk'}\delta_{\sigma\sigma'}$ and $\{\alpha_{k,\sigma}, \gamma_{k',\sigma'}^{\ddagger}\} = \{\alpha_{k,\sigma}, \gamma_{k',\sigma'}\} = \{\gamma_{k,\sigma}, \alpha_{k',\sigma'}^{\ddagger}\} = \{\gamma_{k,\sigma}^{\ddagger}, \alpha_{k',\sigma'}^{\ddagger}\} = 0.$

Integrating out the quasiparticle fields in the partition function, we obtain the effective action

$$S_{\text{eff}} = \frac{2\beta N}{U}|\Delta|^2 - \sum_{k,\sigma,\omega_n}^{\text{BZ}} \ln[\widetilde{\det}(-i\omega_n I + H_{k,\sigma})], \quad (15)$$

where $\widetilde{\det}$ indicates that the zero determinants are excluded. Exclusion of the zero determinant is a direct result in mathematics. The zero determinant requires that both $\text{Re}h_k = 0$ and $\omega_n^2 = (\text{Im}h_k)^2 - |\Delta|^2$ are satisfied simultaneously. For the case in which both relations are satisfied simultaneously, the roots excluded in the sum of ω_n in turn are enclosed in the deformed loop integral, so that some special poles are added in the deformed loop integral. Despite all this, these contributions can be omitted in the thermodynamic limit $N \to \infty$ for k-dependent $\text{Im}h_k$.

Under the saddle point approximation, the functional derivative of the effective action with respect to the auxiliary fields Δ^*, $\partial S_{\text{eff}}/\partial\Delta^* = 0$, yields the trivial solution $\Delta = 0$ and the nontrivial gap equation

$$\frac{4N}{U} = \sum_{k,\sigma}^{\text{BZ}} \frac{\sinh(\beta\Sigma_{k,\sigma})/\Sigma_{k,\sigma}}{\cosh(\beta\text{Re}h_{k,\sigma}) + \cosh(\beta\Sigma_{k,\sigma})}. \quad (16)$$

The condensed energies can then be obtained with $\delta E = \beta^{-1}[S_{\text{eff}}(\Delta) - S_{\text{eff}}(0)]$. Since the integral is a multivalued integral, we define the upper and lower shores of the unanalyzable region. Using the arc theorem, we finally arrive at the explicit form

$$\delta E = \frac{2N}{U}|\Delta|^2 - \frac{1}{\beta}\sum_{k,\sigma}^{\text{BZ}} \ln \frac{1 + \frac{\cosh(\beta\Sigma_{k,\sigma})}{\cosh(\beta\text{Re}h_{k,\sigma})}}{1 + \frac{\cos(\beta\text{Im}h_{k,\sigma})}{\cosh(\beta\text{Re}h_{k,\sigma})}}. \quad (17)$$

The stable saddle point corresponds to a negative δE. Comparing the values of δE for $\Delta \neq 0$ and $\Delta = 0$, the corresponding phase can be determined.

The partition function can be written as

$$\ln \mathcal{Z} \simeq \sum_{k,\sigma,s=\pm}^{\text{BZ}} \ln[1 + \exp(-\beta\varepsilon_s)] - \frac{2\beta N}{U}|\Delta|^2 \quad (18)$$

under the stationary phase approximation [57], where $|\Delta|$ satisfies the gap equation and the negative condensed energies. We prove that the contribution from the second-order correction is zero in Appendix B. It is shown that the second-order contribution produces only a factor of 1 in the partition function. With the partition function $\ln \mathcal{Z}$, the free energy $F = -\beta^{-1}\ln \mathcal{Z}$ can then been obtained. Since complex eigenenergies come in conjugate pairs, the real partition function and thus the free energy are real and objective. From the free energy F, the entropy and specific heat can be calculated straightforwardly using the formulas $S_{\text{en}} = k_B(\ln \mathcal{Z} -$

$\beta\partial \ln \mathcal{Z}/\partial\beta)$ and $\gamma = -\beta\partial S_{\text{en}}/\partial\beta$. It is shown that zero entropy at a temperature approaching to zero is guaranteed. The continuity of these thermodynamic properties can then be analyzed to provide corroborative identification of the orders of various phase transitions. We will use the thermodynamic potential to analyze the continuity of the entropy and specific heat in Sec. III B. Equation (18) and the definition of free energy F show that the continuity of the thermodynamic properties is equivalent to the continuity of the order parameter $|\Delta|$.

III. BILAYER NELSON-HATANO MODEL

A. Spectrum features

To reveal the various phase transitions induced by interaction in disorder-free non-Hermitian systems, we consider the bilayer Nelson-Hatano model in detail. The tight-binding Hamiltonian of the upper layer is given by

$$h_u = \sum_i^N \frac{t}{2}(e^g c_{i+1}^\dagger c_i + e^{-g} c_i^\dagger c_{i+1}), \quad (19)$$

where we have neglected the spin freedom and considered a nonreciprocal hopping. The rightward amplitude is $(t/2)e^g$, while the leftward amplitude is $(t/2)e^{-g}$, and g is determined by the tilt slope of the flux line. In momentum space we have

$$h_u(k) = t(\cosh g \cos ka - i \sinh g \sin ka), \quad (20)$$

where a is the lattice distance. The Hamiltonian of the lower layer $h_l(k)$ takes the same form but with the rightward hopping amplitude $(t/2)e^{-g}$ against the leftward hopping amplitude $(t/2)e^g$. We then have $h_u(k) = h_l^*(k)$.

The spectrum can be obtained: $\varepsilon_{k,\pm}(\Delta) = t\cosh g \cos ka \pm \sqrt{|\Delta|^2 - (t\sinh g \sin ka)^2}$. In the process of the continuous change of the order parameter $|\Delta|$, three critical points, $|\Delta|_{c0}$, $|\Delta|_{c1}$, and $|\Delta|_{c2}$, are identified. As functions of $|\Delta|$, we have access to four different phases via modulation of $|\Delta|$. We label these four different phases as I–IV.

The values of the three critical points are determined as follows. Because $|\Delta|_{c0}$ represents the critical point of the phase transition between nontrivial order ($|\Delta| \neq 0$) and trivial order ($|\Delta| = 0$), $|\Delta|_{c0} = 0$ can be obtained. Corresponding to the transition from Figs. 2(b) to 2(d), the complex-spectrum gap will change from point gapped to gapless. It can be determined by $\max_k^{\text{BZ}}(|\text{Im}\,\varepsilon_{k,\pm}|) = 0$, where $\max_k^{\text{BZ}}(|\text{Im}\,\varepsilon_{k,\pm}|)$ means all k in the BZ and taking the maximum value of $|\text{Im}\,\varepsilon_{k,\pm}|$. Then the critical point $|\Delta|_{c1} = t\sinh g$ is identified. Similarly, separating the gapless phase, phase III [e.g., Fig. 2(d)], from the line-gapped phase, phase IV [e.g., Fig. 2(f)], gives the value of $|\Delta|_{c2}$. At $|\Delta|_{c2}$, the two energy bands exactly intersect; we can then calculate $|\Delta_{c2}|$ using the equation

$$\min_k^{\text{BZ}}[\varepsilon_{k,+}(|\Delta|_{c2})] - \max_k^{\text{BZ}}[\varepsilon_{k,-}(|\Delta|_{c2})] = 0. \quad (21)$$

$|\Delta|_{c2} = t\cosh g$ is obtained straightforwardly. The respective energy spectra of phases I–IV have the following characteristics. Phase I is a normal phase with a zero order parameter $|\Delta| = 0$, and its spectrum is complex and point gapped. In phase II, $0 < |\Delta| < |\Delta|_{c1}$, the spectrum is complex and point gapped [58]. In phase III, $|\Delta|_{c1} < |\Delta| < |\Delta|_{c2}$, the spectrum
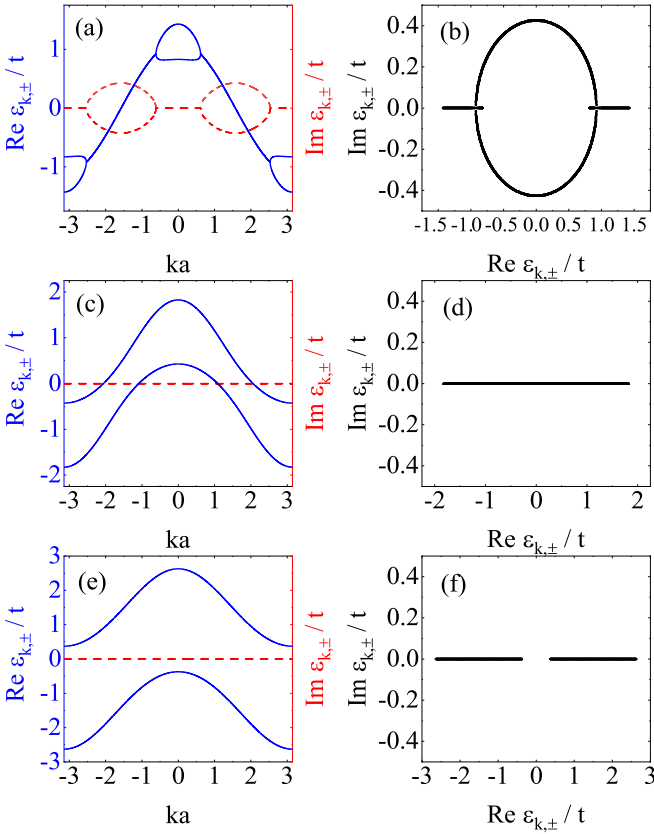
FIG. 2. Spectra for $g = 0.5$. (a), (c), and (e) Energy dispersion relations. (b), (d), and (f) Comparison between the real part and the imaginary part of the spectra. (a) and (b) Phase II, $|\Delta| = 0.3t < t \sinh g$; the spectrum is complex and point gapped. (c) and (d) Phase III, $t \sinh g < |\Delta| = 0.7t < t \cosh g$; the spectrum is purely real and gapless. (e) and (f) Phase IV, $|\Delta| = 1.5t > t \cosh g$; the spectrum is purely real and line gapped.

is real and gapless. In phase IV, $|\Delta| > |\Delta|_{c2}$, the spectrum is real and line gapped [58]. To show the characteristics of phases II, III, and IV, we show the dispersion relations for the real part and imaginary part of the eigenenergy for $g = 0.5$ in Figs. 2(a), 2(c) and 2(e), respectively. The changes in the real part vs the imaginary part are shown in Figs. 2(b), 2(d) and 2(f), respectively.

B. Phase characteristic

The gap equation and condensed energy [Eqs. (16) and (17)] indicate that the order parameter $|\Delta|$ at the critical points $(|\Delta|_{c0}, |\Delta|_{c1}, \text{ and } |\Delta|_{c2})$ depends on the temperature and the strength of the interaction. Therefore, we can obtain the T-U phase diagram. Figure 3(a) is the phase diagram for a fixed value of the non-Hermitian parameter $g(=1.3)$, where the existence of four phases is indicated clearly. There exist two characteristic energy scalings to divide the phase diagram into Hermitian and non-Hermitian parts. One of the characteristic energy scalings is the critical strength of interaction U_c near zero temperature [$\simeq 6t$ in Fig. 3(a)]. It enacts a discontinuous QPT point (QTP) [59]. Another characteristic energy scaling is the non-Hermitian characteristic thermal energy $k_B T_c$ determined by $T_c = t \sinh g / (k_B \pi)$. It corresponds exactly to the

maximum of the imaginary part crossing the first Matsubara frequency [60]. When $T > T_c$ and U deviates from U_c, the system might undergo successive phase transitions IV → III → II → I with increasing temperature. Among them, there is a TCP on the transition line separating phases II and I. At TCP a second-order transition (in orange) and a first-order transition (in green) converge. Both the condensed energy and the order parameter decrease to zero at the TCP. Therefore, this TCP can be determined by $\Delta = 0$ and condensed energy $\delta E = 0$. Figure 3(b) shows that the TCP temperature is $T_{TCP} \simeq 0.66t$ for $g = 1.3$. The order parameter $|\Delta|$ dependence on the temperature is clearly visible in Figs. 3(c) and 3(d). Let us now focus on the transition line between phases I and II. As shown in Fig. 3(c), which embodies the right region of the TCP, $|\Delta|$ changes continuously with temperature, but its derivative has an interruption at $|\Delta| = 0$. This implies that the phase transition occurring in the transition line segment to the right of the TCP is a second-order phase transition. In contrast, in the region to the left of the TCP shown in Fig. 3(d), $|\Delta|$ is continuously modulated in the regime of phases III and II and jumps from a finite value to vanish (or vice versa) at some temperature suddenly as it goes in or out of phase I. This implies that the phase transition occurring in the transition line segment to the left of the TCP is a first-order phase transition. We can make a small expansion near the transition line to obtain a Ginzburg-Landau action, regardless of whether $|\Delta| = 0$ or $\neq 0$. So then we identify them as classical phase transitions.

The phase transitions IV → III → II above the temperature T_c can be clarified as being topological phase transitions because the order parameter and its higher derivative are continuous. Figure 4(a) shows that the entropy S and the specific heat γ are continuous for $|\Delta| \neq 0$. The transition from phase II to phase I contrasts sharply with the phase transitions IV → III → II. It is either second order or first order because the entropy is continuous for $T > T_{TCP}$ and discontinuous for $T < T_{TCP}$, while the specific heats are always discontinuous. We can use the Zak phase [61] to identify the different phases by topological numbers N [62],

$$N = \frac{1}{\pi} \int_0^{\pi/2} dk \frac{\partial}{\partial k} (\arg \varepsilon_+ - \arg \varepsilon_-), \qquad (22)$$

where arg means the angle of the amplitude. That the integration is taken from zero to $\pi/2$ is due to the symmetry with respect to the upper and lower layers. We show the change in N as a function of $|\Delta|$ in Fig. 4(b). It is clearly shown that phases II, III, and IV have different topological numbers. In addition to their topological essence, the phase transition from III to II is a real-complex transition, while the phase transition from IV to III is a real-real transition. Such a real-real transition (III → IV) can be considered a continuous metal-insulator transition corresponding to the energy gap to be closed.

C. QPT and quantum chaotic behavior

The non-Hermitian characteristic temperature T_c is crucial in our discussions. Derived from the spectrum equations discussed above, the imaginary part of the spectrum has a maximum $t \sinh g$. The imaginary part of the spectrum is
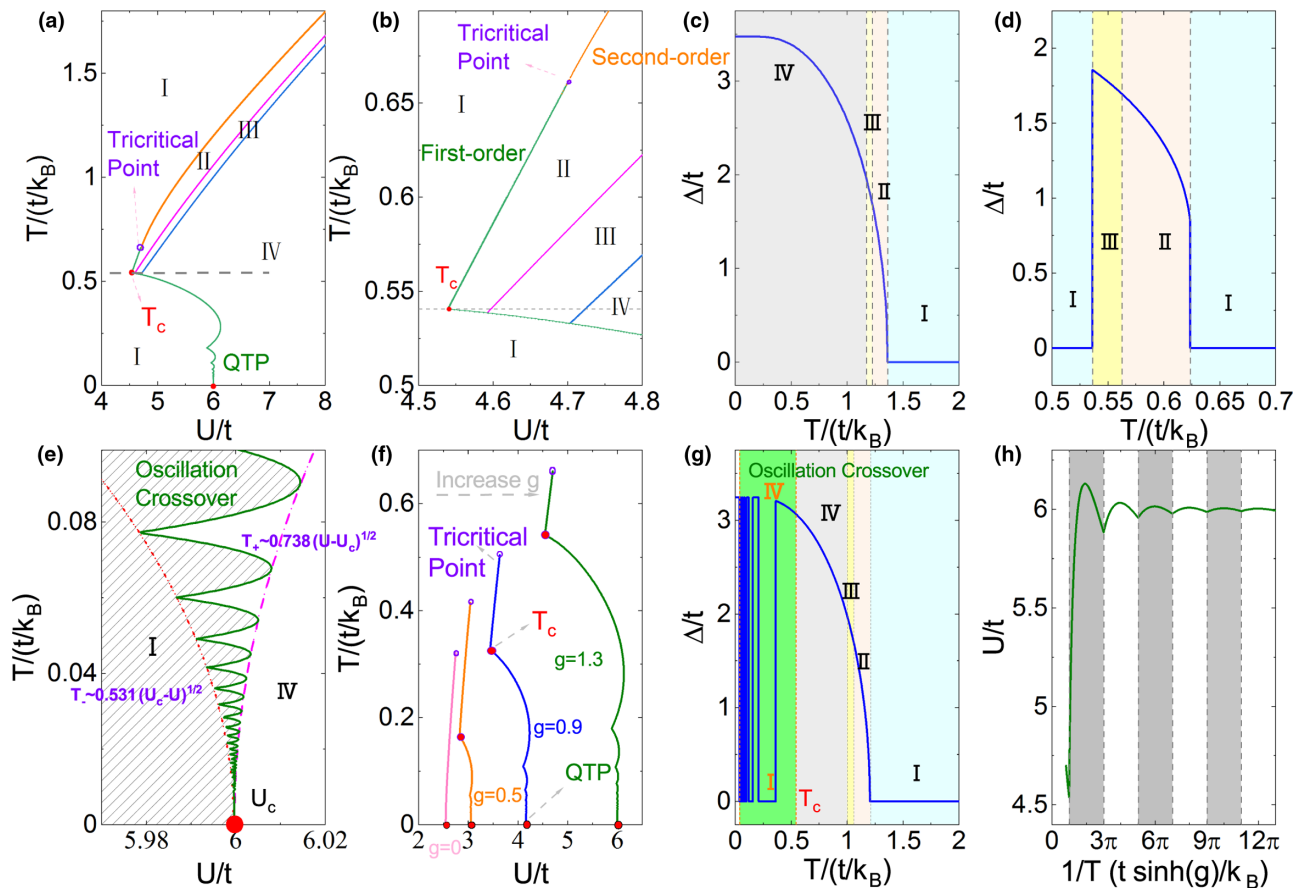
FIG. 3. T-U and Δ-T phase diagrams for $g = 1.3$. (a) Classical and quantum regimes, which are separated by the two characteristic energy scales, U_c and T_c, illustrated in the text, are shown in the phase diagram. The classical phase transition appears at $T > T_c \approx 0.54t$ or U when deviates from $U_c \approx 6t$. Four phases, I–IV, are shown. The TCP is shown on the phase transition line between phases I and II, at which the second-order phase transition line (in orange) connects to the first-order phase transition line (in green). The first-order phase transition appears at $T < T_c$ and U close to U_c. It is a phase transition between a normal phase, phase I, and a line-gapped real-energy phase, phase IV. (b) Enlarged view near the TCP ($k_B T_{\mathrm{TCP}} \sim 0.66t$). (c) Variation of the order parameter $|\Delta|$ vs the temperature in various phases, which are distinguished by dashed lines, to the right of the TCP in the phase diagram in (a). $U = 6.5t$. The transition between phase I and phase II is second order. The order parameter varies continuously with temperature, but its derivative has a singularity at $|\Delta| = 0$. (d) Variation of the order parameter $|\Delta|$ vs the temperature in various phases to the left of TCP in the phase diagram in (a). $U = 4.65t$. The phase transitions between phases I and II and I and III are first order. The order parameter jumps at the temperatures $T \sim 0.54t/k_B$ and $0.62t/k_B$. (e) Enlarged view near the QTP. Two crossover borderlines in the scalings $T_+ \sim 0.738(U - U_c)^{1/2}/k_B$ and $T_- \sim 0.531(U_c - U)^{1/2}/k_B$ divide the phase diagram into three regions, phase I, phase IV, and an oscillation region. (f) The relative changes in T_c, the QTP, and the TCP for several values of g (0, 0.5, 0.9, and 1.3). It is shown that the lager g is, the larger these characteristic parameters are. $T_c = 0$, and the non-Hermitian oscillation region vanishes if $g = 0$. (g) Variation of the order parameter $|\Delta|$ vs the temperature in various phases for $U = 6.002t$. The order parameter shows oscillatory behavior in the region between two crossover borderlines. (h) The non-Hermitian quantum transition line oscillates with a period of $1/T$. The dashed lines are related to the Matsubara frequencies.

associated with the relaxation time of unstable particles τ_s [63]. Therefore, we have

$$\tau_s \geqslant \frac{\hbar}{2t \sinh g} = \frac{\hbar}{2\pi k_B T_c}, \qquad (23)$$

where $k_B T_c = t \sinh g/\pi$. The lower bound on the right side is nothing more than the shortest possible Lyapunov time [64] to reach quantum chaos [32]. For $T > T_c$, $\hbar/(2\pi k_B T_c) \geqslant \hbar(2\pi k_B T)$, the inequality of quantum chaos holds. This regime, in which the rate of dissipation does not exceed the upper bound required by quantum chaos, is viewed as the classical one. However, the characteristic is completely different for $T < T_c$ and U close to U_c. This unique region, resulting

from by non-Hermiticity, is divided into two phases, I and IV, by an oscillating curve in the phase diagram [see Fig. 3(a)].

In contrast, the nonquantum chaos has been presented concretely in the energy spectra. It is seen that for phase II in Fig. 2(b), when we adjust the quantum number k from $-\pi$ to π, eigenvalues $\varepsilon_{k,\pm \mathrm{sign}k}$, i.e., $\varepsilon_{k,\pm}$, cross the real axis to form two closed loops. Mathematically, this is Hopf bifurcation [65]. For phases III and IV in Figs. 2(d) and 2(f), the spectra are real, and there are no exceptional points or bifurcations. This is consistent with the results in Ref. [6], in which the nearest-level-spacing distribution of eigenenergies is a Ginibre one in the complex-eigenenergy phase. Correspondingly, it manifests a Poisson distribution in the real-eigenenergy
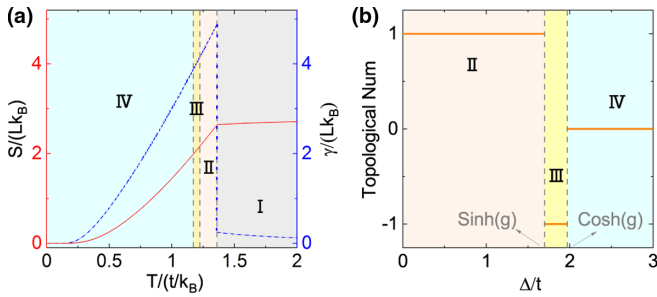
FIG. 4. Properties of the topological phase transition. (a) Entropy and specific heat as a function of temperature for $g = 1.3$ and $U = 6.5t$. Phase transitions IV → III → II are continuous. The phase transition between phases I and II is second order. (b) Topological numbers in phases II, III, and IV. This implies that we can use topological numbers to label different topological phases.

phase. The different distributions correspond to chaotic and nonchaotic ones [66].

To get a closer look, we zoom in on the region around the QTP in Fig. 3(e). It is shown that there are three different regions: phases I and IV and a smooth oscillation crossover region. They are separated by two dashed lines depicted with the same scaling $T_{\pm}(U) \sim |U - U_c|^{1/2}$ but with different coefficients. Excluding some points, for which a crossing does not indicate a phase transition, on the two lines $T_{\pm}(U)$, the clamped extent is the crossover and is similar to the quantum critical region [12]. When we adjust the non-Hermitian parameter g, the QTP shifts [67], as shown in Fig. 3(f). In the limit $g = 0$, $T_c = 0$, and the oscillation region shrinks to zero. Reference [56] pointed out that first-order quantum phase transitions are like quantum critical points with some limitations. We show the typical variation curve of the order parameter $|\Delta|$ vs temperature near the QTP in Fig. 3(g). It is found that the order parameter oscillates between zero and finite values in the crossover region, so that the order parameter $|\Delta|$ is not a certain value at the QTP. We fail to obtain an action similar to Ginzburg-Landau theory. The reason is that the quantum and thermal fluctuations are equally important. Such a feature agrees with the situation in strongly correlated metals [68]. Therefore, we equate this appearance with the non-Hermitian quantum transition.

The characteristics of the oscillation curve remind us of the Shubnikov–de Haas (SdH) oscillation [69] in Hermitian systems. In the presence of a magnetic field B, the quantum oscillation shows a periodicity in $1/B$ at low temperature. This feature is attributed to the Landau quantization of the energy

levels. In Fig. 3(h), we reveal a similar oscillation structure of periodicity at $1/T$ at low temperature. Compared to the magnetic field in the Hermitian system, the non-Hermitian parameter can be viewed as an imaginary magnetic field. This oscillation is attributed to the quantization of the Matsubara frequencies. Meanwhile, the maximum value of the imaginary part of the eigenvalues plays the role of the chemical potential. In Table II, we compare the unquantifiable chaotic oscillation and the SdH oscillation.

IV. CONCLUSIONS

To conclude, we investigated in general the real-complex transition, also called the localization-delocalization transition, in disorder-free non-Hermitian systems with interaction. The phase diagram of various phase transitions and the quantum critical phenomena were revealed by the bilayer Nelson-Hatano model. The relevant characteristic parameters, such as the characteristic temperature for a division of classical and quantum phase transition regimes, the critical strength of interaction, the nontrivial tricritical point, and the relaxation time of unstable particles, were identified. We emphasize a bound of quantum chaos for the quantum critical phenomena determined by the relaxation time and the non-Hermitian parameters. We draw the following conclusions. In the classical regime, the phase transition can be either topological or nontopological. The nontopological transition includes a tricritical point which is the conjunction point of first-order and second-order transition lines. In the quantum regime, it is unquantifiable chaotic, and the first-order phase transition line is an oscillation. The borders of the crossover show 1/2 power law scalings.

ACKNOWLEDGMENTS

APPENDIX A: INTERACTION TERM

In this Appendix, we show that the interaction bringing about real-complex transitions is universal for non-Hermitian systems, whether it is a bilayer system or a monolayer one. However, from the view of interaction, we fucus on bilayer systems because for two reasons; one is the facility to modulate interactions by modulating interlayer distances [71], and the other is that the interaction between excitons at long distances can be attractive [72–74].

TABLE II. Comparison of two oscillation structures.

Hermitian		Non-Hermitian	
Parameter	Symbol	Parameter	Symbol
Magnetic field	**A**	Imaginary magnetic field [1]	$i\mathbf{h}$
Landau levels	$(n + 1/2)\hbar eB/mc$	Matsubara frequencies	$(n + 1/2)2\pi k_B T/\hbar$
Quantum oscillation period [70]	B^{-1}	Crossover oscillation period[a]	T^{-1}
Chemical potential	μ	Maximum imaginary part	$t \sinh g$

[a]See Fig. 3(h).

In monolayer non-Hermitian systems, intralayer terms similar to the interaction of excitons can be found in the Wannier bases. The Coulomb interaction in the Wannier basis is written as

$$H_{\text{Coulomb}} = \frac{1}{2N} \sum_{i,j,i',j',\sigma,\sigma'} U_{ij,i'j'}$$
$$\times c_\sigma^\dagger(\mathbf{r}_i) c_{\sigma'}^\dagger(\mathbf{r}_j) c_{\sigma'}(\mathbf{r}_{j'}) c_\sigma(\mathbf{r}_{i'}). \quad (A1)$$

We stress the mirror term,

$$i + i' = j + j' = L, \quad i \neq j, \quad \sigma = \sigma', \quad (A2)$$

which is different from the contributions of the direct term $i = i' \neq j = j'$ and the exchange term $i = j' \neq j = i'$. We then have

$$H_{\text{mirror}} = \frac{1}{2N} \sum_{i \neq j,\sigma} U_{i,j;L-i,L-j}$$
$$\times c_\sigma^\dagger(\mathbf{r}_i) c_\sigma^\dagger(\mathbf{r}_j) c_\sigma(\mathbf{r}_{L-j}) c_\sigma(\mathbf{r}_{L-i}). \quad (A3)$$

Writing it in k space, it is found that

$$H_{\text{mirror}}$$
$$= \frac{U}{2N} \sum_{i \neq j,\sigma} \frac{1}{N^2} \sum_{\mathbf{k}_1,\mathbf{k}_2,\mathbf{k}_3,\mathbf{k}_4}^{\text{BZ}} e^{-i(\mathbf{k}_1+\mathbf{k}_4)\cdot\mathbf{r}_i}$$
$$\times e^{-i(\mathbf{k}_2+\mathbf{k}_3)\cdot\mathbf{r}_j} c_{\sigma,\mathbf{k}_1}^\dagger c_{\sigma,\mathbf{k}_2}^\dagger c_{\sigma,\mathbf{k}_3} c_{\sigma,\mathbf{k}_4} e^{i(\mathbf{k}_3+\mathbf{k}_4)\cdot\mathbf{L}}$$
$$= \frac{U}{2N} \sum_{\mathbf{k}_1,\mathbf{k}_2,\sigma}^{\text{BZ}} c_{\sigma,\mathbf{k}_1}^\dagger c_{\sigma,\mathbf{k}_2}^\dagger c_{\sigma,-\mathbf{k}_2} c_{\sigma,-\mathbf{k}_1} - \frac{U}{2N} \sum_\sigma$$
$$\times \frac{1}{N} \sum_{\mathbf{k}_1,\mathbf{k}_2,\mathbf{k}_3}^{\text{BZ}} c_{\sigma,\mathbf{k}_1+\mathbf{k}_3}^\dagger c_{\sigma,\mathbf{k}_2-\mathbf{k}_3}^\dagger c_{\sigma,-\mathbf{k}_2} c_{\sigma,-\mathbf{k}_1}. \quad (A4)$$

Here we have used $c_\sigma(\mathbf{r}) = N^{-1/2} \sum_{\mathbf{k}}^{\text{BZ}} e^{i\mathbf{k}\cdot\mathbf{r}} c_{\sigma,\mathbf{k}}$, $c_\sigma^\dagger(\mathbf{r}) = N^{-1/2} \sum_{\mathbf{k}}^{\text{BZ}} e^{-i\mathbf{k}\cdot\mathbf{r}} c_{\sigma,\mathbf{k}}^\dagger$, $N^{-1} \sum_i e^{i(\mathbf{k}_1+\mathbf{k}_2)\cdot\mathbf{r}_i} = \delta_{\mathbf{k}_1+\mathbf{k}_2,0}$, and $e^{i\mathbf{k}\cdot\mathbf{L}} = \exp[i\sum_j(n_j/N_j)\mathbf{b}_j \cdot N_i\mathbf{a}_i] = \exp[i\sum_j(n_j/N_j)N_i 2\pi\delta_{ij}] = 1$. In the thermodynamic limit

H_{mirror} takes the form

$$H_{\text{mirror}} = \frac{U}{2N} \sum_{\mathbf{k}_1,\mathbf{k}_2,\sigma}^{\text{BZ}} c_{\sigma,\mathbf{k}_1}^\dagger c_{\sigma,\mathbf{k}_2}^\dagger c_{\sigma,-\mathbf{k}_2} c_{\sigma,-\mathbf{k}_1}. \quad (A5)$$

This shows that we can use a non-Hermitian monolayer model with the interaction of intralayer excitons to study such real-complex transitions. The contribution of the excitons is crucial for either monolayer or bilayer systems in these non-Hermitian systems.

We adopt the bilayer system in our study. By taking into account only the main hopping terms, we have

$$H_{\text{d}} = -\sum_\sigma \sum_{\mathbf{r}_1,\mathbf{r}_2} \frac{U}{2N} \mathfrak{p}_\sigma^\dagger(\mathbf{r}_1)\mathfrak{p}_\sigma(\mathbf{r}_2) + \text{H.c.}$$
$$= -\frac{U}{N\Omega^2} \sum_\sigma \int d\mathbf{r}_1 d\mathbf{r}_2$$
$$\times c_{\sigma,u}^\dagger(\mathbf{r}_1) c_{\sigma,l}(\mathbf{r}_1) c_{\sigma,l}^\dagger(\mathbf{r}_2) c_{\sigma,u}(\mathbf{r}_2), \quad (A6)$$

where $\mathfrak{p}_\sigma^\dagger$ and $\mathfrak{p}_\sigma$ are the annihilation and creation operators of an interlayer exciton and Ω is the size of the primitive cell. The negative sign means that the order of the operators is exchanged once mathematically in H_{mirror}. Physically, it is due to the dipoles pointing in opposite directions. In k space, it reads

$$H_{\text{d}} = -\frac{U}{N} \sum_{\mathbf{k}_1,\mathbf{k}_2,\sigma}^{\text{BZ}} c_{\mathbf{k}_1,\sigma,u}^\dagger c_{\mathbf{k}_1,\sigma,l} c_{\mathbf{k}_2,\sigma,l}^\dagger c_{\mathbf{k}_2,\sigma,u}. \quad (A7)$$

APPENDIX B: SECOND-ORDER CORRECTION IN THE STATIONARY PHASE APPROXIMATION

Now, we discuss the second-order contribution to $\mathcal{Z}$ under the stationary phase approximation. Usually, the second-order contribution is not zero, as in semiclassical approximations. A nonzero second-order contribution would change the coefficients in front of the propagator. However, such a second-order contribution vanishes. The zero entropy at zero temperature is guaranteed.

We expand $\mathcal{Z}$ near the saddle points Δ_s and Δ_s^* and obtain

$$S_{\text{eff}}(\Delta, \Delta^*) \simeq S_{\text{eff}}(\Delta_s, \Delta_s^*) + \frac{1}{2} (\Delta - \Delta_s \quad \Delta^* - \Delta_s^*) \begin{pmatrix} \frac{\partial^2 S_{\text{eff}}}{\partial\Delta\partial\Delta^*} & \frac{\partial^2 S_{\text{eff}}}{\partial\Delta^{*2}} \\ \frac{\partial^2 S_{\text{eff}}}{\partial\Delta^2} & \frac{\partial^2 S_{\text{eff}}}{\partial\Delta^*\partial\Delta} \end{pmatrix}\Bigg|_{\Delta=\Delta_s} \begin{pmatrix} \Delta^* - \Delta_s^* \\ \Delta - \Delta_s \end{pmatrix}. \quad (B1)$$

The corresponding $\mathcal{Z}$ is given by

$$\mathcal{Z} = \int \frac{d\Delta^* d\Delta}{2\pi i} e^{-S_{\text{eff}}} \simeq e^{-S_{\text{eff}}(\Delta_s,\Delta_s^*)} \int \frac{d\delta\Delta^* d\delta\Delta}{2\pi i} \exp\left[-\frac{1}{2}(\delta\Delta \quad i\delta\Delta^*) \begin{pmatrix} \frac{\partial^2 S_{\text{eff}}}{\partial\Delta\partial\Delta^*} & i\frac{\partial^2 S_{\text{eff}}}{\partial\Delta^{*2}} \\ -i\frac{\partial^2 S_{\text{eff}}}{\partial\Delta^2} & \frac{\partial^2 S_{\text{eff}}}{\partial\Delta^*\partial\Delta} \end{pmatrix}\Bigg|_{\Delta=\Delta_s} \begin{pmatrix} \delta\Delta^* \\ -i\delta\Delta \end{pmatrix}\right]. \quad (B2)$$

With the substitutions

$$\begin{pmatrix} \delta\Delta^* \\ -i\delta\Delta \end{pmatrix} = \begin{pmatrix} 1 & -i \\ -i & 1 \end{pmatrix} \begin{pmatrix} \text{Re}\delta\Delta \\ \text{Im}\delta\Delta \end{pmatrix}$$

and $(1/2\pi i)\int d\delta\Delta^* d\delta\Delta = (1/\pi)\int d\text{Re}\delta\Delta d\text{Im}\delta\Delta$, Eq. (B2) becomes

$$\mathcal{Z} = 2\exp\left\{-S_{\text{eff}}(\Delta_s, \Delta_s^*) - \frac{1}{2}\ln\left[\widetilde{\det}\begin{pmatrix} \frac{\partial^2 S_{\text{eff}}}{\partial\Delta\partial\Delta^*} & i\frac{\partial^2 S_{\text{eff}}}{\partial\Delta^{*2}} \\ -i\frac{\partial^2 S_{\text{eff}}}{\partial\Delta^2} & \frac{\partial^2 S_{\text{eff}}}{\partial\Delta^*\partial\Delta} \end{pmatrix}\Bigg|_{\Delta=\Delta_s}\right]\right\} \quad (B3)$$

after integrating $\delta\Delta$, where $\widetilde{\det}$ means that we get rid of those values making the determinant zero. Utilizing the effective action and the eigenenergies

$$S_{\text{eff}} = \frac{2\beta N}{U}|\Delta|^2 - \sum_{\mathbf{k},\sigma}^{\text{BZ}} \sum_{j=1}^{2} \ln\left[1 + \exp\left(-\beta z_j\right)\right] \tag{B4}$$

and $z_{1,2} = \text{Re}h_{\mathbf{k}} \pm \sqrt{|\Delta|^2 - (\text{Im}h_{\mathbf{k}})^2}$, the relations are easy to find: $\partial z_j/\partial\Delta^* = \pm\Delta/[2\sqrt{\Delta\Delta^* - (\text{Im}h_{\mathbf{k}})^2}]$, $\partial z_j/\partial\Delta = \pm\Delta^*/[2\sqrt{\Delta\Delta^* - (\text{Im}h_{\mathbf{k}})^2}]$, $\partial^2 z_j/\partial\Delta^2 = \mp\Delta^{*2}/\{4[\Delta\Delta^* - (\text{Im}h_{\mathbf{k}})^2]^{3/2}\}$, $\partial^2 z_j/\partial\Delta^{*2} = \mp\Delta^2/\{4[\Delta\Delta^* - (\text{Im}h_{\mathbf{k}})^2]^{3/2}\}$, and $\partial^2 z_j/\partial\Delta^*\partial\Delta = \pm[\Delta\Delta^* - 2(\text{Im}h_{\mathbf{k}})^2]/\{4[\Delta\Delta^* - (\text{Im}h_{\mathbf{k}})^2]^{3/2}\}$. The matrix in Eq. (B2) can be expressed as

$$\begin{pmatrix} \frac{\partial^2 S_{\text{eff}}}{\partial\Delta\partial\Delta^*} & i\frac{\partial^2 S_{\text{eff}}}{\partial\Delta^{*2}} \\ -i\frac{\partial^2 S_{\text{eff}}}{\partial\Delta^2} & \frac{\partial^2 S_{\text{eff}}}{\partial\Delta^*\partial\Delta} \end{pmatrix} = \beta \begin{pmatrix} \frac{2N}{U} + \sum_{\mathbf{k},\sigma,j}^{\text{BZ}} \frac{\frac{\partial^2 z_j}{\partial\Delta\partial\Delta^*} - \beta\frac{\partial z_j}{\partial\Delta^*}\frac{\partial z_j}{\partial\Delta}\frac{1}{1+e^{-\beta z_j}}}{1+e^{\beta z_j}} & i\sum_{\mathbf{k},\sigma,j}^{\text{BZ}} \frac{\frac{\partial^2 z_j}{\partial\Delta^{*2}} - \beta\left(\frac{\partial z_j}{\partial\Delta^*}\right)^2 \frac{1}{1+e^{-\beta z_j}}}{1+e^{\beta z_j}} \\ -i\sum_{\mathbf{k},\sigma,j}^{\text{BZ}} \frac{\frac{\partial^2 z_j}{\partial\Delta^2} - \beta\left(\frac{\partial z_j}{\partial\Delta}\right)^2 \frac{1}{1+e^{-\beta z_j}}}{1+e^{\beta z_j}} & \frac{2N}{U} + \sum_{\mathbf{k},\sigma,j}^{\text{BZ}} \frac{\frac{\partial^2 z_j}{\partial\Delta\partial\Delta^*} - \beta\frac{\partial z_j}{\partial\Delta^*}\frac{\partial z_j}{\partial\Delta}\frac{1}{1+e^{-\beta z_j}}}{1+e^{\beta z_j}} \end{pmatrix}. \tag{B5}$$

The determinant in Eq. (B3) is found as

$$\widetilde{\det}\begin{pmatrix} \frac{\partial^2 S_{\text{eff}}}{\partial\Delta\partial\Delta^*} & i\frac{\partial^2 S_{\text{eff}}}{\partial\Delta^{*2}} \\ -i\frac{\partial^2 S_{\text{eff}}}{\partial\Delta^2} & \frac{\partial^2 S_{\text{eff}}}{\partial\Delta^*\partial\Delta} \end{pmatrix} = \widetilde{\det}\begin{pmatrix} \frac{\partial^2 S_{\text{eff}}}{\partial\Delta\partial\Delta^*} & \frac{\Delta^{*2}}{|\Delta|^2}\frac{\partial^2 S_{\text{eff}}}{\partial\Delta^{*2}} \\ \frac{\Delta^2}{|\Delta|^2}\frac{\partial^2 S_{\text{eff}}}{\partial\Delta^2} & \frac{\partial^2 S_{\text{eff}}}{\partial\Delta^*\partial\Delta} \end{pmatrix} = \widetilde{\det}\begin{pmatrix} \frac{\partial^2 S_{\text{eff}}}{\partial\Delta\partial\Delta^*} - \frac{\Delta^2}{|\Delta|^2}\frac{\partial^2 S_{\text{eff}}}{\partial\Delta^2} & \frac{\Delta^{*2}}{|\Delta|^2}\frac{\partial^2 S_{\text{eff}}}{\partial\Delta^{*2}} - \frac{\partial^2 S_{\text{eff}}}{\partial\Delta^*\partial\Delta} \\ \frac{\Delta^2}{|\Delta|^2}\frac{\partial^2 S_{\text{eff}}}{\partial\Delta^2} & \frac{\partial^2 S_{\text{eff}}}{\partial\Delta^*\partial\Delta} \end{pmatrix}. \tag{B6}$$

Because

$$\frac{\partial^2 S_{\text{eff}}}{\partial\Delta\partial\Delta^*} - \frac{\Delta^2}{|\Delta|^2}\frac{\partial^2 S_{\text{eff}}}{\partial\Delta^2} = \frac{2\beta N}{U} + \frac{\beta}{2}\sum_{\mathbf{k},\sigma}^{\text{BZ}}\sum_{j=1}^{2} \frac{3 - 2j}{\sqrt{\Delta\Delta^* - (\text{Im}h_{\mathbf{k}})^2}(1 + e^{\beta z_j})}$$

$$= -\frac{\beta}{2}\left[-\frac{4N}{U} + \sum_{\mathbf{k},\sigma}^{\text{BZ}} \frac{\sinh(\beta\sqrt{|\Delta|^2 - (\text{Im}h_{\mathbf{k}})^2})/\sqrt{\Delta\Delta^* - (\text{Im}h_{\mathbf{k}})^2}}{\cosh\left(\beta\text{Re}h_{\mathbf{k}}\right) + \cosh(\beta\sqrt{|\Delta|^2 - (\text{Im}h_{\mathbf{k}})^2})}\right], \tag{B7}$$

it is shown that $[\partial^2 S_{\text{eff}}/\partial\Delta\partial\Delta^* - (\Delta^2/|\Delta|^2)\partial^2 S_{\text{eff}}/\partial\Delta^2]_{\Delta_s=0} = 0$ using the gap equation [Eq. (16)]. Together with its conjugate, we have proved that the second-order correction to the stationary phase approximated partition function is zero.

---

[1] N. Hatano and D. R. Nelson, Localization Transitions in Non-Hermitian Quantum Mechanics, Phys. Rev. Lett. **77**, 570 (1996).

[2] N. Hatano and R. N. David, Non-Hermitian delocalization and eigenfunctions, Phys. Rev. B **58**, 8384 (1998).

[3] J. Feinberg and A. Zee, Non-Hermitian localization and delocalization, Phys. Rev. E **59**, 6433 (1999).

[4] K. B. Efetov, Directed Quantum Chaos, Phys. Rev. Lett. **79**, 491 (1997).

[5] A. V. Kolesnikov and K. B. Efetov, Localization-Delocalization Transition in Non-Hermitian Disordered Systems, Phys. Rev. Lett. **84**, 5600 (2000).

[6] R. Hamazaki, K. Kawabata, and M. Ueda, Non-Hermitian Many-Body Localization, Phys. Rev. Lett. **123**, 090603 (2019).

[7] K. Kawabata and S. Ryu, Nonunitary Scaling Theory of Non-Hermitian Localization, Phys. Rev. Lett. **126**, 166801 (2021).

[8] P. W. Anderson, Absence of diffusion in certain random lattices, Phys. Rev. **109**, 1492 (1958).

[9] J. Billy, V. Josse, Z. Zuo, A. Bernard, B. Hambrecht, P. Lugan, D. Clement, L. Sanchez-Palencia, P. Bouyer, and A. Aspect, Direct observation of Anderson localization of matter waves in a controlled disorder, Nature (London) **453**, 891 (2008).

[10] A. Smith, J. Knolle, D. L. Kovrizhin and R. Moessner, Disorder-Free Localization, Phys. Rev. Lett. **118**, 266601 (2017).

[11] J. A. Hertz, Quantum critical phenomena, Phys. Rev. B **14**, 1165 (1976).

[12] S. Sachdev, *Quantum Phase Transitions* (Cambridge University Press, Cambridge, 2011).

[13] P. Gegenwart, Q. Si, and F. Steglich, Quantum criticality in heavy-fermion metals, Nat. Phys. **4**, 186 (2008).

[14] C. M. Varma, Pseudogap Phase and the Quantum-Critical Point in Copper-Oxide Metals, Phys. Rev. Lett. **83**, 3538 (1999).

[15] D. E. Sheehy and J. Schmalian, Quantum Critical Scaling in Graphene, Phys. Rev. Lett. **99**, 226803 (2007).

[16] S. Coleman and E. Weinberg, Radiative corrections as the origin of spontaneous symmetry breaking, Phys. Rev. D **7**, 1888 (1973).

[17] D. Belitz and T. R. Kirkpatrick and T. Vojta, How generic scale invariance influences quantum and classical phase transitions, Rev. Mod. Phys. **77**, 579 (2005).

[18] T. Goto, Y. Shindo, H. Takahashi, and S. Ogawa, Magnetic properties of the itinerant metamagnetic system $Co(S_{1-x}Se_x)_2$ under high magnetic fields and high pressure, Phys. Rev. B **56**, 14019 (1997).

[19] M. Uhlarz, C. Pfleiderer, and S. M. Hayden, Quantum Phase Transitions in the Itinerant Ferromagnet ZrZn$_2$, Phys. Rev. Lett. **93**, 256404 (2004).

[20] V. Taufour, D. Aoki, G. Knebel, and J. Flouquet, Tricritical Point and Wing Structure in the Itinerant Ferromagnet, Phys. Rev. Lett. **105**, 217201 (2010).

[21] A. Antoniazzi, D. Fanelli, S. Ruffo, and Y. Y. Yamaguchi, Nonequilibrium Tricritical Point in a System with Long-Range Interactions, Phys. Rev. Lett. **99**, 040601 (2007).

[22] R. B. Griffiths, Thermodynamics near the Two-Fluid Critical Mixing Point in He^3-He^4, Phys. Rev. Lett. **24**, 715 (1970).

[23] A. Aharony, Tricritical points in systems with random fields, Phys. Rev. B **18**, 3318 (1978).

[24] C. M. Bender and S. Boettcher, Real Spectra in Non-Hermitian Hamiltonians Having $\mathcal{PT}$ Symmetry, Phys. Rev. Lett. **80**, 5243 (1998).

[25] A. Mostafazadeh, Pseudo-Hermitian representation of quantum mechanics, Int. J. Geom. Methods Mod. Phys. **7**, 1191 (2010).

[26] Y. Ashida, Z. Gong, and M. Ueda, Non-Hermitian physics, Adv. Phys. **69**, 249 (2020).

[27] G. Gamow, Zur quantentheorie des atomkernes, Z. Phys. **51**, 204 (1928).

[28] H. Feshbach, A unified theory of nuclear reactions. II, Ann. Phys. (NY) **19**, 287 (1962).

[29] S. Hartnoll, Theory of universal incoherent metallic transport, Nat. Phys. **11**, 54 (2015).

[30] A. Legros, S. Benhabib, W. Tabis, F. Laliberté, M. Dion, M. Lizaire, B. Vignolle, D. Vignolles, H. Raffy, Z. Z. Li, P. Auban-Senzier, N. Doiron-Leyraud, P. Fournier, D. Colson, L. Taillefer, and C. Proust, Universal T-linear resistivity and Planckian dissipation in overdoped cuprates, Nat. Phys. **15**, 142 (2019).

[31] F. G. Scholtz, H. B. Geyer, and F. J. W. Hahne, Quasi-Hermitian operators in quantum mechanics and the variational principle, Ann. Phys. (NY) **213**, 74 (1992).

[32] J. Maldacena, S. H. Shenker, and D. Stanford, A bound on chaos, J. High Energ. Phys. 08 (2016) 106.

[33] A. M. Garcia-Garcia, Y. Jia, D. Rosa, and J. J. M. Verbaarschot, Dominance of Replica Off-Diagonal Configurations and Phase Transitions in a $\mathcal{PT}$ Symmetric Sachdev-Ye-Kitaev Model, Phys. Rev. Lett. **128**, 081601 (2022).

[34] J. E. Golub, S. D. Baranovskii, and P. Thomas, Evidence for Dipole-Dipole Hopping of GaAs Quantum Well Excitons, Phys. Rev. Lett. **78**, 4261 (1997)

[35] S. Yao and Z. Wang, Edge States and Topological Invariants of Non-Hermitian Systems, Phys. Rev. Lett. **121**, 086803 (2018).

[36] F. Song, S. Yao, and Z. Wang, Non-Hermitian Skin Effect and Chiral Damping in Open Quantum Systems, Phys. Rev. Lett. **123**, 170401 (2019).

[37] L. Xiao, T. Deng, K. Wang, G. Zhu, Z. Wang, W. Yi, and P. Xue, Non-Hermitian bulk ¨C boundary correspondence in quantum dynamics, Nat. Phys. **16**, 761 (2020).

[38] N. Okuma, K. Kawabata, K. Shiozaki, and M. Sato, Topological Origin of Non-Hermitian Skin Effects, Phys. Rev. Lett. **124**, 086801 (2020).

[39] L. Li, C. H. Lee, S. Mu, and J. Gong, Critical non-Hermitian skin effect, Nat. Commun. **11**, 5491 (2020).

[40] D. Zou, T. Chen, W. He, J. Bao, C. H. Lee, H. Sun, and X. Zhang, Observation of hybrid higher-order skin-topological ef-fect in non-Hermitian topolectrical circuits, Nat. Commun. **12**, 7201 (2021).

[41] N. Okuma and M. Sato, Quantum anomaly, non-Hermitian skin effects, and entanglement entropy in open systems, Phys. Rev. B **103**, 085428 (2021).

[42] M. Lu, X. X. Zhang, and M. Franz, Magnetic Suppression of Non-Hermitian Skin Effects, Phys. Rev. Lett. **127**, 256402 (2021).

[43] S. Longhi, Non-Hermitian skin effect beyond the tight-binding models, Phys. Rev. B **104**, 125109 (2021).

[44] X. Sun, P. Zhu, and T. L. Hughes, Geometric Response and Disclination-Induced Skin Effects in Non-Hermitian Systems, Phys. Rev. Lett. **127**, 066401 (2021).

[45] J. P. Eisenstein and A. H. MacDonald, Bose-Einstein conden-sation of excitons in bilayer electron systems, Nature (London) **432**, 691 (2004).

[46] L. V. Keldysh, Coulomb interaction in thin semiconductor and semimetal films, Sov. JETP Lett. **29**, 658 (1979).

[47] P. Cudazzo, I. V. Tokatly, and A. Rubio, Dielectric screening in two-dimensional insulators: Implications for excitonic and impurity states in graphane, Phys. Rev. B **84**, 085406 (2011).

[48] F. Wu, F. Qu, and A. H. Macdonald, Exciton band structure of monolayer, Phys. Rev. B **91**, 075310 (2015).

[49] J. W. Negele and O. Henri, *Quantum Many-Particle Systems* (CRC Press, Boca Raton, FL, 2018).

[50] B. Gardas, S. Deffner, and A. Saxena, Non-Hermitian quantum thermodynamics, Sci. Rep. **6**, 23408 (2016).

[51] V. Jakubsky, Thermodynamics of pseudo-Hermitian systems in equilibrium, Mod. Phys. Lett. A **22**, 1075 (2007).

[52] R. Arouca, C. H. Lee, and C. M. Smith, Unconventional scaling at non-Hermitian critical points, Phys. Rev. B **102**, 245145 (2020)

[53] X. Z. Zhang and Z. Song, Probing the superfluid-insulator phase transition by a non-Hermitian external field, Phys. Rev. B **104**, 094301 (2021).

[54] K. Yamamoto, M. Nakagawa, K. Adachi, K. Takasan, M. Ueda, and N. Kawakami, Theory of Non-Hermitian Fermionic Su-perfluidity with a Complex-Valued Interaction, Phys. Rev. Lett. **123**, 123601 (2019).

[55] A. Mostafazadeh, Pseudo-Hermiticity versus PT symmetry: The necessary condition for the reality of the spectrum of a non-Hermitian Hamiltonian, J. Math. Phys. **43**, 205 (2002)

[56] T. E. Lee and C. K. Chan, Heralded Magnetism in Non-Hermitian Atomic Systems, Phys. Rev. X **4**, 041001 (2014).

[57] J. R. Klauder, Path integrals and stationary-phase approxima-tions, Phys. Rev. D **19**, 2349 (1979).

[58] K. Kawabata, K. Shiozaki, M. Ueda, and M. Sato, Symme-try and Topology in Non-Hermitian Physics, Phys. Rev. X **9**, 041015 (2019).

[59] C. Pfleiderer, Why first order quantum phase transitions are interesting, J. Phys.: Condens. Matter **17**, S987 (2005).

[60] Y. Wang, A. Abanov, B. L. Altshuler, E. A. Yuzbashyan, and A. V. Chubukov, Superconductivity near a Quantum-Critical Point: The Special Role of the First Matsubara Frequency, Phys. Rev. Lett. **117**, 157001 (2016).

[61] J. Zak, Berry's Phase for Energy Bands in Solids, Phys. Rev. Lett. **62**, 2747 (1989).

[62] H. Shen, B. Zhen, and L. Fu, Topological Band Theory for Non-Hermitian Hamiltonians, Phys. Rev. Lett. **120**, 146402 (2018).

[63] S. Das Sarma and F. Stern, Single-particle relaxation time versus scattering time in an impure electron gas, Phys. Rev. B **32**, 8442(R) (1985).

[64] S. H. Shenker and D. Stanford, Black holes and the butterfly effect, J. High Energ. Phys. 03 (2014) 067.

[65] J. E. Marsden and M. McCracken, *The Hopf Bifurcation and Its Applications* (Springer, New York, NY, 2012)

[66] Z. E. Rudnick, What is quantum chaos, Not. Am. Math. Soc. **55**, 32 (2008).

[67] Y. Ashida and M. Ueda, Multiparticle quantum dynamics under real-time observation, Phys. Rev. A **95**, 022124 (2017).

[68] T. Senthil, L. Balents, S. Sachdev, A. Vishwanath, and M. P. A. Fisher, Quantum criticality beyond the Landau-Ginzburg-Wilson paradigm, Phys. Rev. B **70**, 144407 (2004).

[69] L. Schubnikow and W. J. De Haas, A new phenomenon in the change of resistance in a magnetic field of single crystals of bismuth, Nature (London) **126**, 500 (1930).

[70] D. Shoenberg, *Magnetic Oscillations in Metals* (Cambridge University Press, Cambridge, 2009).

[71] A. Ciarrocchi, F. Tagarelli, A. Avsar, and A. Kis, Excitonic devices with van der Waals heterostructures: Valleytronics meets twistronics, Nat. Rev. Mater. **7**, 449 (2022).

[72] V. M. Agranovich and B. S. Toshich, Collective properties of Frenkel excitons, Sov. Phys. JETP **26**, 104 (1968).

[73] R. M. Lee, N. D. Drummond, and R. J. Needs, Exciton-exciton interaction and biexciton formation in bilayer systems, Phys. Rev. B **79**, 125308 (2009).

[74] D. J. Choksy, C. Xu, M. M. Fogler, L. V. Butov, J. Norman, and A. C. Gossard, Attractive and repulsive dipolar interaction in bilayers of indirect excitons, Phys. Rev. B **103**, 045126 (2021).